

# Idealized tracer transport models with time-varying transport: applications to ocean boundary currents

F. Terenzi · Timothy M. Hall

Received: 24 November 2008 / Accepted: 17 May 2009 / Published online: 9 June 2009  
© Springer Science+Business Media B.V. 2009

**Abstract** One-dimensional advection–diffusion and advection–diffusion–dilution (or “leaky-pipe”) models have been widely used to interpret a variety of geophysical phenomena. For example, in the ocean these tools have been used to interpret the penetration and spreading of tracers such as Chlorofluorocarbons (CFCs) along the Deep Western boundary current (DWBC). Usually, the transport coefficients of such models are taken to be constant in time, thus assuming the transport to be in steady state. Here, we relax this assumption and calculate tracer-signal variability in two simple 1D models for the boundary current having low-amplitude time-varying coefficients. Given a background tracer gradient due, for example, to a steady-state source in a boundary region, the resulting tracer field exhibits fluctuations due to the transport acting on the gradients. We compare the transport-induced tracer fluctuations to propagated fluctuations occurring in steady-state models with a periodic source in the boundary region. Using coefficients fitted to DWBC tracer observations, we find that in the North Atlantic propagated tracer fluctuations are larger, while in the sub-tropics transport-induced fluctuations dominate. This contrasts a common view that subtropical and tropical DWBC fluctuations in tracers such as CFCs, temperature and salinity anomalies are propagated signals from the northern formation region. However, the predicted transport-induced fluctuations in these models are still smaller than the observed fluctuations.

**Keywords** Ocean tracer transport · Deep-western boundary current · Idealized analytic models

---

F. Terenzi (✉) · T. M. Hall  
Department of Applied Physics and Applied Mathematics, Columbia University, New York,  
NY 10027, USA  
e-mail: ft2104@columbia.edu

T. M. Hall  
NASA Goddard Institute for Space Studies, New York,  
NY 10025, USA

## 1 Introduction

One-dimensional (1D) advection–diffusion and advection–diffusion–dilution (or “leaky-pipe”) models are common idealized descriptions of tracer transport used in a wide variety of geophysical domains. In the atmosphere, New and Plumb [13] defined and solved the “Tropical Leaky Pipe” (TLP), an advection–dilution model for stratospheric transport, which explained features of the mean-age distribution present both in observations and in more complex 2D and 3D models by adding a dilution term to the 1D advection–diffusion idealized model by Plumb [15]. Mote et al. [11] obtained improved estimates of vertical diffusion and horizontal mixing by fitting CH<sub>4</sub> and H<sub>2</sub>O data to a 1D advection–diffusion–dilution model of the tropical stratosphere. Also, in the context of stratospheric transport, Hall and Waugh [7] computed the TLP residence time and analyzed its relationship to mean-age. In the troposphere, McKenna [9] used similar concepts to explain the dilution of pollution plumes.

In ocean applications, tracer transport along isopycnals [18] and anthropogenic carbon [e.g., 6] have been addressed with the use of 1D advection–diffusion models. Idealized models have also been exploited in order to interpret the propagation of tracer signals that enter the DWBC in the North-Atlantic (NA) formation regions and propagate along the DWBC into the deep tropics [3, 5, 14, 16, 21]. In particular, these models were used to interpret anomalies of tracers such as temperature ( $T$ ) and salinity ( $S$ ), as well as to explain discrepancies among measured and modeled velocity fields. It was recognized that differences among velocity estimates are due to mixing and recirculation. More recently, Mouchet and Deleersnijder [12] used a 1D advection–diffusion model, in which the deep ocean is represented as a leaky pipe with a decreasing cross section (i.e. a leaky funnel), allowing recirculation of water and tracers toward the surface, in order to study the ventilation rate in the ocean as simulated by a 3D GCM.

Advection–diffusion and advection–dilution analytical models are highly simplified, kinematic descriptions of complex fluid flow and tracer transport. Nonetheless, they offer a convenient interpretation of tracer measurements and an efficient way to explore the sensitivity of tracers to bulk parameters of the flow, which cannot be easily tuned independently in 3D numerical models. In all analyses that we know of, transport coefficients of such models are taken to be constant; that is, the transport is assumed to be in a steady state. This is warranted if the time-averaged behavior is stationary, but it precludes the analysis of certain classes of tracer signals if the transport fluctuates, as we describe below.

In this work we generalize common 1D advection–diffusion and advection–dilution models to include fluctuations in transport coefficients. Our focus is the NA DWBC, and our primary goal is to compare and contrast two mechanisms for fluctuations in tracer concentration: (1) local generation due to fluctuations in transport acting on background tracer gradients; and (2) propagation of tracer fluctuations generated in northern source regions. The effects of mechanism 2 can be accommodated using constant transport coefficients, while mechanism 1 requires time-varying coefficients.

The motivation for comparing these mechanisms is observations of temporal variations in tracers such as CFCs and  $T$  and  $S$  in the DWBC. CFCs enter the DWBC in NA source regions, and their propagation along the DWBC is a valuable diagnostic of transport. A number of studies have had success constraining advection–dilution and advection–diffusion models with CFC measurements [14, 16, 17, 21]. On the other hand, Steinfeldt and Rhein [17], who analyzed repeated measurements of CFC-11 and CFC-12 in the western tropical Atlantic from 1990 to 2002, observed fluctuations in concentrations that they could not explain using an analysis with constant transport rates. Several studies [2, 4, 8, 10] have interpreted subtropical and tropical DWBC  $T$  and  $S$  fluctuations as signals propagated from the northern source

regions, where they are generated by variability in air–sea interactions. However, using an advection–dilution model with constant coefficients tuned to CFC and helium–tritium observations, Waugh and Hall [21] were not able to replicate  $T$  and  $S$  fluctuations. Their analysis indicated that fluctuations propagated from northern source regions should be attenuated beyond detection in the subtropics. Could tracer fluctuations such as these be generated by mechanism 1, transport fluctuations acting on background gradients?

A second goal of our study is to provide solutions to ubiquitous models in the case of time-varying transport that may be applicable to a wide range of tracer analyses. A third goal is to compare and contrast advection–dilution and advection–diffusion models in the case of temporally varying coefficients.

This paper is organized as follows: In Sect. 2 we define both the advection–dilution and advection–diffusion models and compare and contrast their behavior. In Sect. 3, results for both models are discussed for two cases: (1) periodic fluctuations in transport with linearly increasing boundary conditions (BCs) and (2) steady-state transport with periodic BCs. A comparison of CFC observational data and predictions by both models is presented in Sect. 3.3. Finally, a discussion of the main findings of this study follows in Sect. 4. Details on the derivations of the main analytical solutions can be found in the Appendices.

## 2 Model descriptions

We extend idealized advection–diffusion and advection–dilution 1D models to include small temporal variations in the transport coefficients. Both models can be represented in vector form as:

$$\begin{aligned} \frac{\partial}{\partial t} \mathbf{c} + (1 + \epsilon f(t)) \mathbf{L}(\mathbf{c}) &= 0 \\ \mathbf{c}(x, 0) &= 0 \\ \mathbf{c}(0, t) &= \mathbf{y}(t), \end{aligned} \tag{1}$$

where  $\mathbf{c} = \mathbf{c}(x, t)$  is the tracer concentration (units tracer mass per unit mass),  $\mathbf{L}$  is the steady-state transport operator,  $\epsilon$  is the dimensionless perturbation parameter ( $\epsilon \ll 1$ ), and  $f(t)$  is a dimensionless time-dependent function of order one, which summarizes time-variation in transport. Here we consider the case in which a passive tracer penetrates the ocean by air–sea gas exchange at the sea surface. This process, along with transport near the surface, sets a near-surface concentration, that is assumed to be known. This is the boundary condition, BC, at  $x = 0$ . Initial conditions are applied at all  $x > 0$ .

### 2.1 1 D Advection–diffusion model

The BC sets a signal that is transported into the domain by a constant uniform flow along an isopycnal that extends indefinitely in the positive  $x$  direction and by diffusive isopycnal mixing. The diffusion coefficient  $k$  is positive, and the bulk advection  $u$  is non-negative. The transport operator in Eq. (1) is:

$$L = u \frac{\partial}{\partial x} + k \frac{\partial^2}{\partial x^2} \tag{2}$$

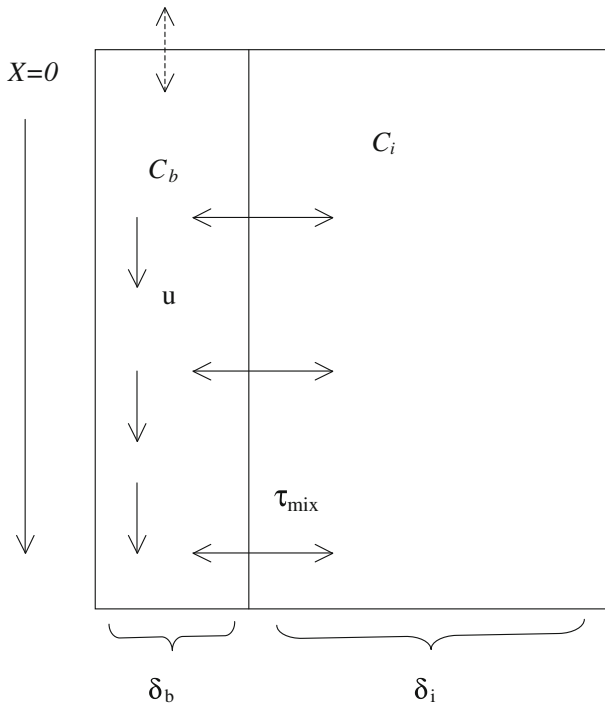


**Fig. 1** Schematic of the “leaky-pipe” boundary-current model [21]. The model consists of two coupled one-dimensional semi-infinite domains: a boundary-current core region, “b”, with uniform along velocity  $u$  and cross-sectional area  $\delta_b$ , and a larger interior region, “i”, with cross-sectional area  $\delta_i$  and no flow. The cross sectional area of the core to interior region is the ratio  $\alpha = \delta_b/\delta_i$ . Tracer concentrations mix relaxationally between the two regions at a rate  $\sigma = \tau_{\text{mix}}^{-1}$ .  $c_b(x, t)$  and  $c_i(x, t)$  are the tracer concentrations in the boundary current and interior region, respectively

### 2.2 1 D Boundary-current model (“leaky pipe”)

Following Waugh and Hall [21] we define an idealized boundary-current model that consists of two coupled one-dimensional semi-infinite domains: a boundary-current core region with uniform along-stream (positive) velocity  $u$  and a stationary surrounding interior ocean region (see illustration in Fig. 1). Tracer concentrations mix relaxationally between the two regions at a rate  $\sigma = 1/\tau_{\text{mix}}$ , where  $\tau_{\text{mix}}$  is a relaxational time scale. Along-flow diffusion is neglected, as scaling arguments show that is much slower than lateral mixing [14]. As already mentioned, similar models have been used in previous studies for extracting transport rates from tracer observations [3, 14], although generally in these models the surrounding interior has been assumed to be an infinite reservoir. We now have to keep track of tracers in two regions: the interior region “i” and the boundary region “b”. The vector that represents the tracer concentration  $\mathbf{c}$  is:

$$\mathbf{c} = \begin{cases} c_b \\ c_i \end{cases} \tag{3}$$

The transport operator in Eq. (1) can be written as:

$$\mathbf{L} = \begin{pmatrix} u \frac{\partial}{\partial x} + \sigma & -\sigma \\ -\alpha\sigma & \alpha\sigma \end{pmatrix} \tag{4}$$

where  $\alpha$  is the cross-sectional area ratio of the core region to the surrounding interior region.

### 2.3 Physical model comparison

Although their domains of application sometimes overlap, the two models are structurally different and fitted coefficients must be interpreted distinctly. In oceanographic applications the 1D advection–diffusion model has often been used to summarize transport along 2D thermocline isopycnals. In this context the model velocity may only be related to a physical current velocity if the model is applied locally along a streamline of 2D flow. In such an application the along-flow diffusivity would crudely represent the effects of mixing across streamlines. If the model is applied to represent the cross-basin averaged transport away from the outcrop, then the coefficients have no simple interpretation, and the model is merely a convenient two-parameter form that empirically describes tracer transport better than either pure diffusion or pure bulk advection. The advection–dilution model of boundary currents is more physical structurally, in that the model velocity can be identified with the velocity along the fluid plume, if many simplifying assumptions are made. The relaxation time-scale represents crudely the mixing between the boundary and the much larger surrounding regions. The two models can produce similar tracer distributions (the interior region of the advection–dilution model redistributes tracer of core-origin to different regions of the boundary, similar to the effects of along-flow mixing), but the best-fit coefficients will not be the same.

### 2.4 Perturbation solutions

In order to solve Eq. (1) analytically, we perform a perturbation of order  $O(\epsilon)$ ; that is, we consider solutions of the form  $\mathbf{c} = \mathbf{c}^{(0)} + \epsilon\mathbf{c}^{(1)}$ . Eq. (1) is thus separated into zero-th and first-order components, both of which can be solved analytically. In the spirit of idealized models we choose a periodic transport perturbation  $f = \text{Re}(e^{i\omega t})$ , capturing one component of the spectrum of variations. (Subsequently, we examine the sensitivity to  $\omega$ .) For the BC we choose a linear increase,  $y(t) = \gamma t$ , crudely representing the history of anthropogenic tracers such as CFCs and industrial  $\text{CO}_2$  for at least parts of their histories. (Linear is chosen over exponential because it simplifies the solutions greatly.) The zero-th and first-order solutions can be written as

$$\mathbf{c}^{(0)}(x, t) = \gamma(t - \Gamma(x)) \tag{5}$$

and

$$\mathbf{c}^{(1)}(x, t) = \mathbf{A}^{(1)}(x) \cos\left(\omega\left(t - \tau^{(1)}(x)\right)\right), \tag{6}$$

where  $\Gamma$  is the mean transit time [20],  $\tau^{(1)}$  is the phase lag and  $A^{(1)}$  is the amplitude (Appendix A).

### 2.5 Parameter values

The parameter values used to perform the calculations for both models are reported in Table 1. The values for the boundary-current model are chosen in order to be consistent with the study of Waugh and Hall [21]. Waugh and Hall [21] showed that the parameter combination:

**Table 1** Parameter values used in the calculations for the two models

Model	$u$ [cm <sup>2</sup> /s]	$\tau_{\text{mix}}$ [years]	$k$ [m <sup>2</sup> /s]	$\gamma$ [tracer unit/year]	$\alpha$	$T_p$ [years]
Boundary current	5	1	–	1	0.1	10
		10	–			
		$\infty$	–			
Advection–diffusion	0.5	–	$10^{-7}$	1	–	10
		–	$10^2$			
		–	$10^3$			

$u = 5 \text{ cm s}^{-1}$ ,  $\alpha = 0.1$  and  $\tau_{\text{mix}} = 1$  year for the boundary-current model gives a good agreement to a range of tracer observations. For the advection–diffusion model, we chose  $u = 0.5 \text{ cm s}^{-1}$ , the value indicated by [21]. This choice results in an agreement between  $\Gamma = x/u$ , the mean transit time for the advection–diffusion model, and  $\Gamma$  in the boundary region of the advection–dilution model,

$$\Gamma = \tau_{\text{adv}} \left( 1 + \frac{1}{\alpha} \right). \tag{7}$$

Waugh and Hall [21] also found an upper bound for the diffusion coefficient of  $k \sim 10^4 \text{ m}^2 \text{ s}^{-1}$ . The high value of  $k$  and the small value of  $u$  are probably due to the fact that the large along-flow diffusion contributes to the tracer propagation, as also noticed in other studies (e.g., [17]). Here we span a wide range of diffusivities (from  $10^{-7}$  to  $10^3 \text{ m}^2 \text{ s}^{-1}$ ) to allow for different regimes and document sensitivity. The highest value of  $k$  in our range is the “standard” value, equal to the value used by Steinfeldt and Rhein [17], which is more realistic than the low value. The low value is well within the weak mixing limit. (Note that  $k$  cannot be set to zero identically because the solutions are singular.) The rate of linear increase of the tracer at the origin is  $\gamma = 1$  tracer unit per year. The perturbation magnitude is  $\epsilon = 1/3$ . The period of transport oscillations,  $T_p = 2\pi/\omega$ , is 10 years. In what follows, it is understood that the parameters used are those presented in this section, unless otherwise stated. Sensitivity to the choice of some of the parameters is also shown in Sect. 3.

### 3 Results and discussion

#### 3.1 Periodic fluctuations in transport

The increasing boundary condition establishes background gradients in tracer concentration upon which the transport fluctuations act. Shown in Fig. 2 is the tracer’s time series at a fixed location ( $x \sim 8,000 \text{ km}$ ) for the boundary component of the boundary-current model. Not surprisingly, the amplitude of the induced fluctuations depends on the dilution coefficient  $\tau_{\text{mix}}$ . Fig. 3 shows the profiles of the amplitude,  $\epsilon A_1(x)$ , and phase lag,  $\tau_1(x)$ , as a function of non-dimensional distance  $x$ , with transport oscillation period  $T_p = 10$  years. The dilution coefficients for the boundary-current model are:  $\tau_{\text{mix}} = \infty$  years (red),  $\tau_{\text{mix}} = 10$  years (black) and  $\tau_{\text{mix}} = 1$  year (blue). The diffusion coefficients for the advection–diffusion model are:  $k = 10^{-7} \text{ m}^2 \text{ s}^{-1}$  (red),  $10^2 \text{ m}^2 \text{ s}^{-1}$  (black) and  $10^3 \text{ m}^2 \text{ s}^{-1}$  (blue). Dimensionless distance  $x$  is defined as the ratio of the physical position along the DWBC current to the distance,  $uT_p$ , a parcel of water with speed  $u$  would cover in time  $T_p$ . For  $T_p = 10$  years and  $u = 5 \text{ cm s}^{-1}$ , this distance is  $\sim 16,000 \text{ km}$ . Thus, for the advection–dilution model with these parameter

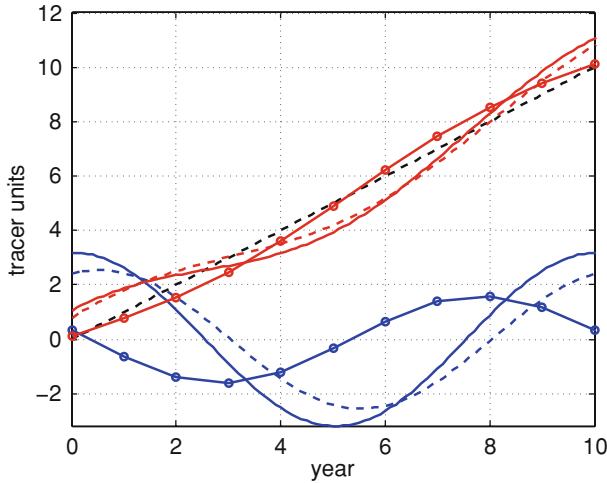


**Fig. 2** Tracer concentration time series for the boundary-current model at a fixed location,  $x = 8,000$  km: zero-th order solution  $c_0(t)$  (black solid line); first order solution  $\epsilon \cdot c_1(t)$  (blue lines) and full solution  $c(t) = c_0(t) + \epsilon \cdot c_1(t)$  (red lines). The advective velocity is  $u = 5 \text{ cm s}^{-1}$ . Solutions for different values of the dilution coefficient are plotted with different symbols:  $\tau_{\text{mix}} = \infty$  (solid line),  $\tau_{\text{mix}} = 10$  years (dash) and  $\tau_{\text{mix}} = 1$  year (circles)

values, only the early part of the first amplitude cycle can be realized physically. (For example, Steinfeldt and Rhein [17] report that for Labrador Sea Water the pathway from the Labrador Sea to  $16^\circ\text{N}$  is about 8,500 km, and the pathway to  $10^\circ\text{S}$  is 13,000 km. The authors define the distance from the source region as the shortest pathway following the DWBC along the coast line.)

The amplitude and phase profiles in the two models behave similarly. The  $x$  structure in both models attenuates with distance from the source and with increasing mixing. We give a physical interpretation of the behavior of both  $\epsilon A_1(x)$  and  $\tau_1(x)$  for the boundary-current model, as simpler analytical expressions can be found for this model. The curves of Fig. 3a and b illustrate two noteworthy limits, weak and strong mixing via large and small  $\tau_{\text{mix}}$  (small and large  $\sigma$ ).

First, consider the weak mixing limit:

$$\sigma \ll \frac{u}{x} \left( \frac{\omega^2 + \alpha^2 \sigma^2}{\omega^2} \right) \tag{8}$$

The amplitude becomes:

$$A_b^{(1)} \sim \sqrt{2} \frac{\gamma}{\omega} \left( 1 - \cos \left( \frac{\omega \beta + x}{u} \right) \right)^{1/2} \tag{9}$$

(see Eq. (27) in Appendix). In this limit, the amplitude oscillates in  $x$ ; that is, the tracer fluctuation magnitude is modulated by an envelope with periodic structure in  $x$  (red curve, Fig. 3a). At short distances from the origin, the boundary current has only had time to experience one phase of the transport perturbation. The further into the domain the water travels, the more time it spends in this phase and the greater the tracer perturbation. Consequently, the amplitude increases with  $x$ . However, water at  $x > uT_p/2$  has been in the domain long enough to also experience the opposite phase of the transport perturbation, which cancels

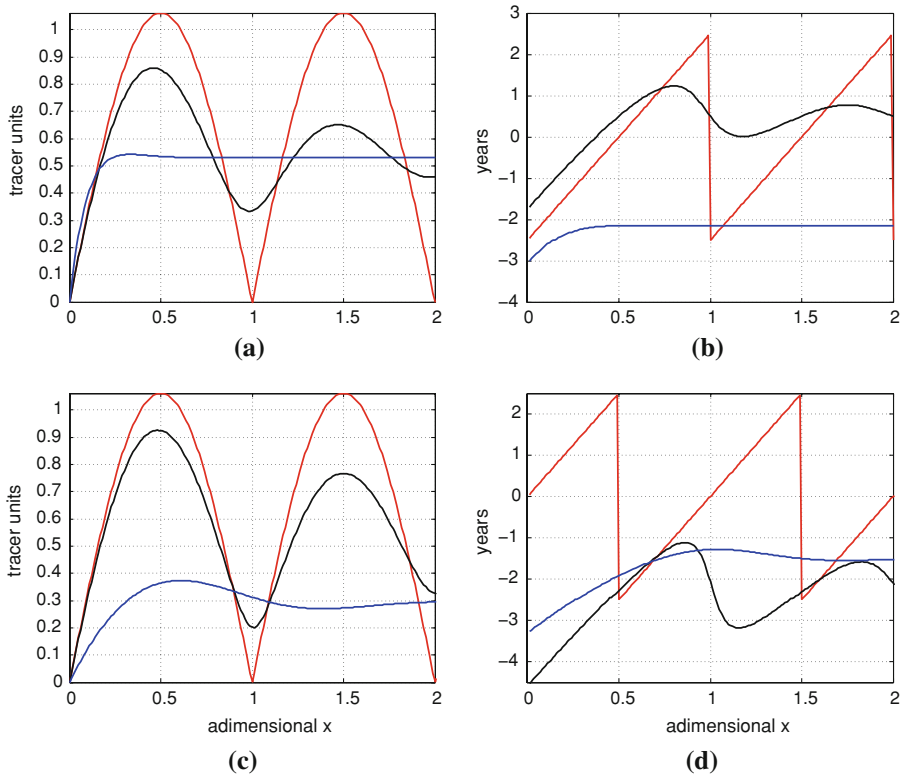


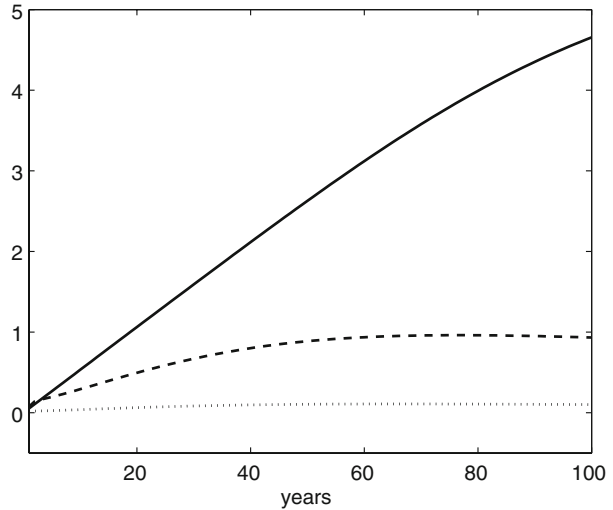
**Fig. 3** The  $x$ -dependence of (a) amplitude  $\epsilon A^{(1)}$  for the boundary-current model; (b) phase lag  $\tau^{(1)}$  for the boundary-current model; (c) amplitude  $\epsilon A^{(1)}$  for the advection–diffusion model, and (d) phase lag  $\tau^{(1)}$  for the advection–diffusion model. For the boundary-current model the dilution coefficients are:  $\tau_{\text{mix}} = \infty$  (red),  $\tau_{\text{mix}} = 10$  year (black) and  $\tau_{\text{mix}} = 1$  year (blue). For the advection–diffusion model, the diffusion coefficients are:  $k = 10^{-7} \text{ m}^2 \text{ s}^{-1}$  (red),  $k = 10^2 \text{ m}^2 \text{ s}^{-1}$  (black) and  $k = 10^3 \text{ m}^2 \text{ s}^{-1}$  (blue). Other parameters are  $T_p = 10$  years,  $\gamma = 1$  tracer unit year $^{-1}$ , and  $u = 5 \text{ cm s}^{-1}$  and  $u = 0.5 \text{ cm s}^{-1}$  for the boundary-current and the advection–diffusion model, respectively. Distance  $x$  is non-dimensionalized by the length scale  $uT_p$

the effect of the first phase, and the amplitude decreases with  $x$ . At  $x = uT_p$ , the effects on the tracer of the two phases exactly cancel, and the amplitude is zero. For  $x > uT_p$  the cycle repeats.

In the strong mixing limit, on the other hand, water at  $x$  has a wide range of times since boundary contact, because of the possibility of a wide range of times spent in the interior region “en route” to  $x$ . Consequently, there is a wide range of phase of the transport perturbation and the net effect is cancellation and the loss of spatial structure in amplitudes. In this limit the tracer perturbation amplitude is simply determined by the amount of time the transport perturbation acts on the background tracer trend, i.e.,  $A_b^{(1)} \sim \gamma/\omega$ . The mixing rate,  $\sigma$ , required to be in this limit,  $\sigma \gg u/x$ , depends on  $x$ . For small  $x$ , there has been little time since boundary contact for mixing to act, so that the mixing rate must be greater to be in this limit. This limit is illustrated by the blue curve in Fig. 3a for non-dimensional  $x \sim 0.3$ , which corresponds to  $x \sim 5,000 \text{ km}$ ,  $\sigma \gg 1 \cdot 10^{-8} \text{ s}^{-1}$ , or  $\tau_{\text{mix}} \ll 3$  years.

Similar arguments apply to the phase-lag time,  $\tau^{(1)}(x)$ . Consider the unmixed case. The tracer perturbation at  $x$  results from integrating the transport perturbation over the time

**Fig. 4** Amplitude  $\epsilon A^1$  of transport-induced fluctuations for the boundary-current model versus the period of transport oscillations  $T_p$  for  $x = [10^2, 10^3, 10^4]$  km (dotted, dashed and solid lines, respectively).  $\tau_{\text{mix}} = 1$  year, while all other parameters are as in Table 1. Dimensions are tracer units



required to advect the unmixed parcel to  $x$  from the origin, namely,  $x/u$ . As  $x$  increases, the integration time increases, and an increasingly large range of perturbation phases have been sampled. The resulting average tracer phase becomes increasingly different from the contemporaneous transport phase; that is,  $\tau^{(1)}(x)$  increases with  $x$ . However, at  $x = uT_p$ , all transport phases have been equally sampled, the phase is indistinguishable from that at  $x = 0$ , and the cycle repeats. In the strong mixing limit, this argument only applies at small  $x$ . Once an  $x$  is reached so that  $\sigma \gg u/x$ , then there is a wide range of transit times, and the net result is a lack of any further  $x$ -dependence of  $\tau^{(1)}$ . In this limit,

$$\tau_b^{(1)} \sim -\frac{1}{\omega} \tan^{-1} \left( \frac{2\sigma\omega(\omega^2 + \alpha^2\sigma^2 + \alpha\sigma^2)}{\sigma^2\omega^2 - (\omega^2 + \alpha^2\sigma^2 + \alpha\sigma^2)^2} \right), \tag{10}$$

is dependent on  $\sigma$  and  $\alpha$ , but not  $x$ . Similar arguments apply for the advection–diffusion model for both the amplitude and the phase lag (Fig. 3c, d). The difference is that for advection–diffusion the range of transit times in the well-mixed limit is due to the 1D random-walk in the flow direction, rather than the range of times spent in any external reservoir (the interior region).

We show in Fig. 4 the dependence of the tracer-fluctuation amplitude on the forcing period,  $T_p$ , for  $\tau_{\text{mix}} = 1$  year at three different  $x$ . Three features are clear. (1) At small  $T_p$  the amplitude increases linearly with  $T_p$ . In this regime the magnitude of a tracer fluctuation is simply determined by the time over which the transport fluctuation acts on the background gradient. The more time in one phase, the greater the tracer perturbation. (2) At large  $T_p$  the amplitude is independent of  $T_p$ . In this limit, the effect of the transport fluctuation on the tracer gradient has saturated. The variation of the transport is now so slow that, over the entire range of times it takes fluid to reach  $x$  from the origin, the transport phase is approximately constant. In this limit, the transport perturbation is equivalent to a slow modulation of the background transport rates, the tracer distribution is in approximate equilibrium with these rates, and zero-order equations suffice to represent the system. (3) The  $T_p$  at the transition from one limit to the other increases with  $x$ . Larger  $x$  corresponds to longer transit times to arrive at  $x$ , and, hence, slower transport fluctuations are required to be in the saturated limit. In other words, as  $x$  increases at constant

$T_P$ , more phase variation of the transport fluctuation is experienced en route to  $x$  from the origin.

Finally, we note that there are other limits for the amplitude and phase not discussed here. The general dependence on the three time-scales,  $T_P$ ,  $\tau_{\text{mix}}$ , and the advective time  $\tau_{\text{adv}} = x/u$ , results in a rich variety of behavior. Here, we have explored only the behavior that is plausibly relevant to analyses of the DWBC. In other applications other regimes may be more relevant.

### 3.2 Comparison of tracer-fluctuation mechanisms

In this section we compare two distinct mechanisms to generate temporal fluctuations in tracer concentration: (1) fluctuations in transport acting on background tracer gradients due to a steady source, and (2) fluctuations in tracer source causing fluctuations in concentration in the source region, which are then propagated downstream by steady transport.

Mechanism 1 has been examined above with our two idealized models. To examine mechanism 2 we use the same models, but now with steady transport ( $\epsilon = 0$ ) and a periodic boundary condition on tracer concentration applied at the origin. Solutions can be written  $c(x, t) = P(x) \cos(\omega_*(t - \phi(x)))$ , where  $\omega_*$  is the boundary condition frequency. Expressions for  $P(x)$  and  $\phi(x)$  are found in Appendix C. To compare fluctuating tracer mechanisms, we set  $\omega_*$  to the frequency of the periodic transport fluctuation of mechanism 1; that is,  $\omega_* = \omega = 2\pi/10$  years. This is reasonable if the same mode of climate variability (e.g., the North-Atlantic Oscillation) is the origin for both the transport fluctuation and the source-region air–sea exchange fluctuation. For concreteness, we also set the mechanism 2 source-region amplitude,  $P(0) = \gamma T_P$ . This equality is not crucial. As we shall see, at some point downstream, mechanism 1 become larger than mechanism 2. The smaller  $P(0)$  is, the closer to the origin this crossover point occurs.

Figures 5a and c show the  $x$  profiles of the two mechanisms' transport fluctuation amplitudes,  $P$  and  $\epsilon A^{(1)}$ , for the two models. The mixing rates are  $\tau_{\text{mix}} = 1$  year,  $k = 10^3 \text{ m}^2 \text{ s}^{-1}$ , and other parameters are as in Fig. 2. Waugh and Hall [21] found that these parameters could reproduce observed tracer distributions in the DWBC. In both models  $P$  decreases exponentially with  $x$ , while  $\epsilon A^{(1)}$  increases from zero and asymptotes to constant values,  $\sim 0.5$  for the boundary current model and  $\sim 0.3$  for the advection–diffusion model. Fig. 5b and d show the ratios  $\epsilon A^{(1)}/P$  as functions of  $x$  for the two models. In both models, mechanism 2 (propagated fluctuations) dominates tracer fluctuations at small  $x$  and mechanism 1 (in situ transport-generated fluctuations) dominates at large  $x$ . For the boundary-current model, the crossover point where  $\epsilon A^{(1)} = P$  is  $x \approx 4,500$  km, while for the advection–diffusion model it is  $x \approx 3,000$  km. To examine further parameter sensitivity of these crossover points we contour in Fig. 6 the ratio  $\epsilon A^{(1)}/P$  of the boundary-current model against the boundary current speed,  $u$ , and the mixing timescale,  $\tau_{\text{mix}}$ , evaluated at the position  $x = 15,000$  km. Slower current speed and more rapid mixing favor transport-induced fluctuations (mechanism 2), while faster current speed and less mixing favor propagated fluctuations (mechanism 1).

The crossover distances 3,000 km (advection–diffusion) and 4,500 km (boundary current) are both less than the distance along the DWBC from the Labrador Sea to the subtropics. We conclude that in the subtropics tracer fluctuations induced by transport fluctuations dominate over fluctuations propagated from North-Atlantic source regions, for a class of tracers with sufficiently large background gradients. The question to which we now turn is whether these fluctuations can explain certain observed subtropical fluctuations.

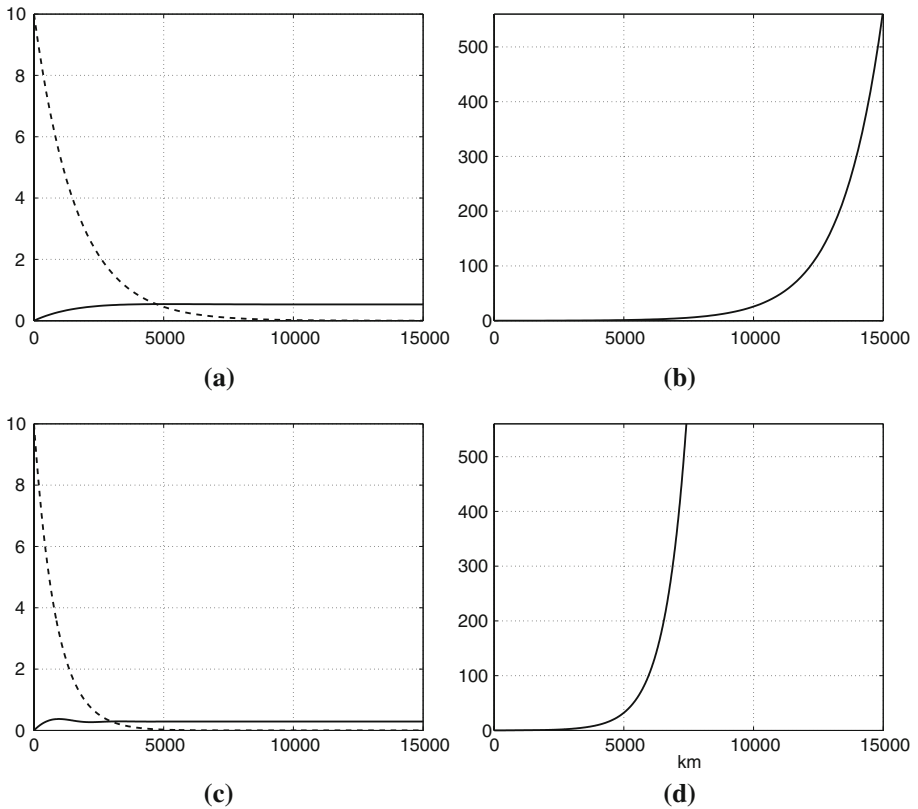
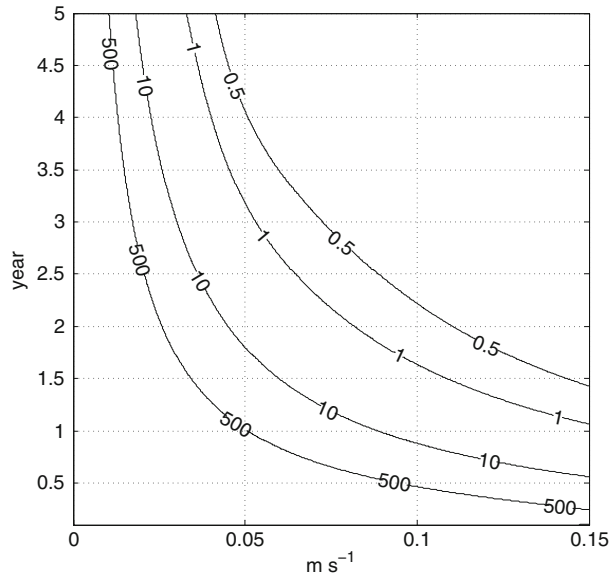


**Fig. 5** (a) The amplitudes in the boundary current model,  $\epsilon A^1$ , of transport-induced fluctuations (*solid black*) and  $P$  of a tracer-signal propagating in response to periodic variation in boundary condition at  $x = 0$  (*dashed black*); (b) The ratio  $\epsilon A^1/P$  for the boundary current model; (c) and (d) equivalent to (a) and (b) for the advection–diffusion model. For the boundary-current model  $\tau_{\text{mix}} = 1$  year and for the advection–diffusion model  $k = 10^3 \text{ m}^2 \text{ s}^{-1}$ . Other parameters as in Fig. 3. The propagated tracer’s amplitude at  $x = 0$  is 10 tracer units, and its period of oscillation is 10 years, identical to the period of transport variation

### 3.3 Relation to observations

Steinfeldt and Rhein [17] present and analyze a series of CFC-11 and CFC-12 measurements in the western tropical Atlantic within the period 1990–2002. Here, we analyze their CFC-11 at two sites: “44°W”, a transect straddling the equator at 44°W, and “10°S”, a transect running about 5° east from 35°W at approximately 10°S (see Fig. 2 of [17]). Observed CFC-11 core concentrations for three NADW components and their standard deviations are shown in black in Fig. 7. The three NADW components are: LSW (Labrador Sea Water), ULSW (Upper LSW) and LNADW (Lower NADW). On average, CFC-11 increases in time at all sites and water masses, and Steinfeldt and Rhein [17] are able to capture well this increase by fitting a 1D advection–diffusion model—the same presented here in the unperturbed case—forced by boundary conditions at the remote northern outcrops. In addition to the overall increase, however, there are fluctuations, particularly the post-2000 decline seen in ULSW and LNADW. Steinfeldt and Rhein [17] note that these fluctuations cannot be captured by

**Fig. 6** Ratio between the amplitudes of transport-induced fluctuation,  $\epsilon A^1$ , and periodic amplitude,  $P$ , at  $x = 15,000$  km versus  $u$  and  $\tau_{\text{mix}}$  for the boundary-current model. Other parameters as in Fig. 3



the steady model, and it is these fluctuations that we attempt to explain with our non-steady boundary-current model.

Also shown in Fig. 7 are model time series evaluated at values of  $x$  equal to the distance along the boundary current from the northern outcrop to the observational site. These values are 11,000 km to the  $44^\circ\text{W}$  site and 13,000 km to the  $10^\circ\text{S}$  site for ULSW/LSW and 2,500 km longer to each site for LNADW (Reiner Steinfeldt, personal communications). The blue curve corresponds to the steady-state model, with “best-value” parameters from Waugh and Hall [21]:  $\tau_{\text{mix}} = 1$  year,  $\alpha = 0.1$ , and  $u = 5$  cm s $^{-1}$ . The linear increase,  $\gamma$ , is set to match the linear trend over the time span shown in each panel. The solid red curve is the “best-estimate” fluctuating solution, using the same parameters as steady state and, in addition, a transport oscillation period of  $T_p = 10$  years. The value of  $T_p$  is somewhat arbitrary, and in reality a spectrum of transport fluctuations is present. Here, our goal is merely to determine the plausibility of a decadal-scale transport-fluctuation mechanism. Our choice of 10 years allows us to focus on interannual variability but is significantly shorter than the time-scale that has established the background CFC gradient ( $\sim 60$  years). The observed fluctuations in Fig. 7, although poorly resolved by the infrequent measurements, suggest periods between 6 and 12 years. The perturbation magnitude for the “best-estimate” case is  $\epsilon = 1/3$ ; i.e., as large as possible, but still comfortably consistent with the linearization. The dashed red curve is the “envelope-pushed” solution to maximize the fluctuating tracer amplitude, in which  $\tau_{\text{mix}} = 3$  years, the largest value still roughly consistent with Waugh and Hall [21], and  $\epsilon = 1/2$ , pushing the limit of linearity.

There is no model-observational agreement in detail, nor should any be expected, as we have not attempted to model any particular fluctuation in transport (for example, some observed fluctuation in DWBC core velocity). Moreover, even aside from disagreement in detail, our model cannot match the magnitude of post-2000 CFC-11 decline in concentration at  $10^\circ\text{S}$  in ULSW and LNADW. The smaller observed fluctuations at  $44^\circ\text{W}$  for all water masses and  $10^\circ\text{S}$  for LSW have magnitudes that can roughly be matched by the model with “envelope-pushed” parameters. It may be that the observed fluctuations are the result of a

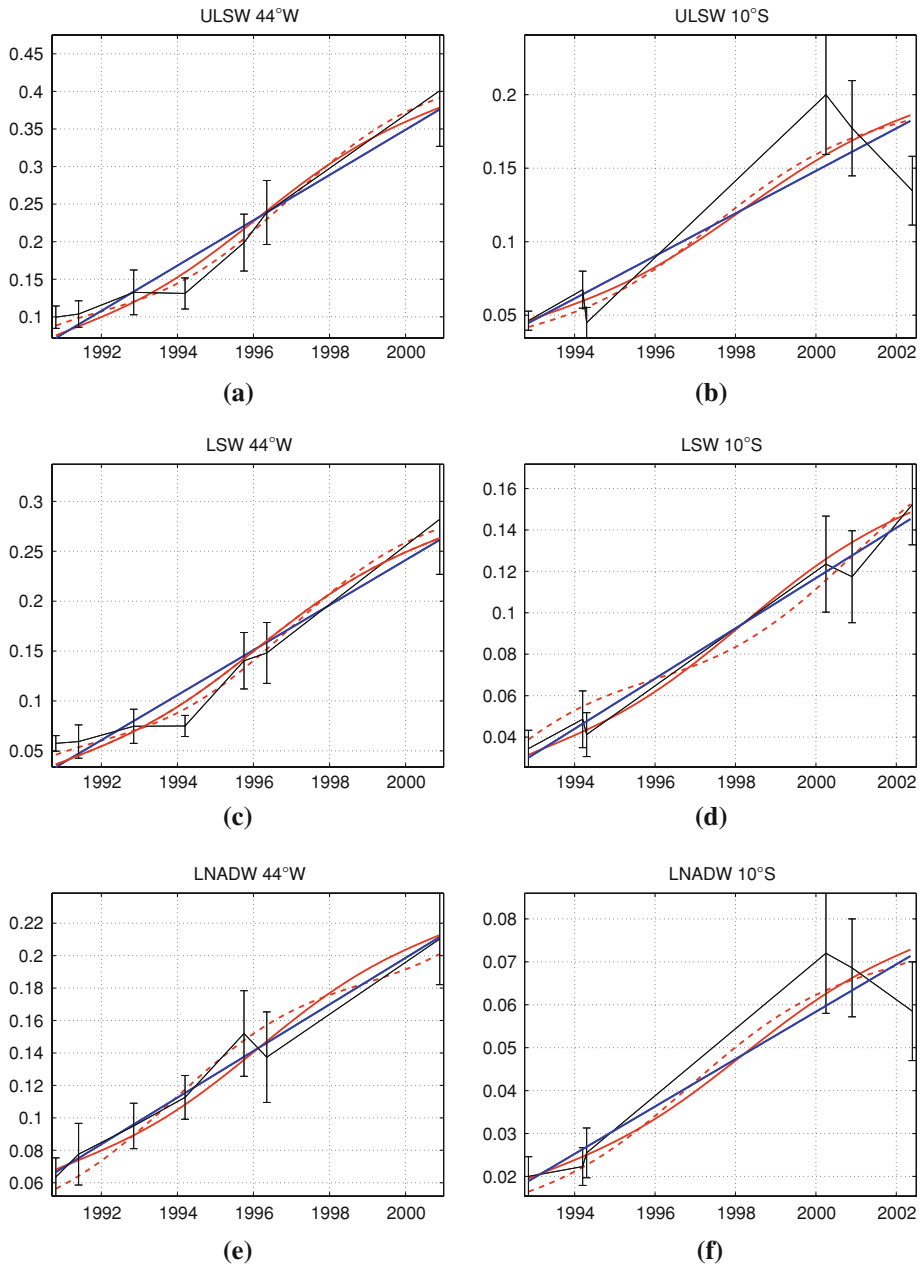


**Fig. 7** Comparison between measured and modeled CFC-11 concentrations at stations “44°W” and “10°S”. Observed core concentrations for ULSW, LSW and NADW components and their standard deviations for the period 1990–2002 are shown in black (data from [17]). Blue lines represent the zero-order solution  $c_0(x, t)$  of the boundary-current model, assuming linear increase for the boundary condition, and red lines represent the total perturbed solution up to first-order,  $c = c_0(x, t) + \epsilon \cdot c_1(x, t)$ . The period of transport oscillation is  $T_p = 10$  years. Red solid lines correspond to “best-estimate” choice of parameters ( $\tau_{\text{mix}} = 1$  year,  $\epsilon = 1/3$ ), and red dashed correspond to  $\tau_{\text{mix}} = 3$  years and  $\epsilon = 1/2$ . See text for details on the adopted values of  $x$  and  $u$ . Units are in picomole  $\text{kg}^{-1}$

complete different mechanism, the intermittent measurements sampling eddies that carry water from outside the DWBC into the domain of observation. This water would have very different CFC concentration. Such a process is well beyond the scope of the simple boundary current model, in which the bulk-averaged effect of such eddies is summarized by a single mixing time-scale. The time-variation of our model's coefficients can only be expected to replicate slow modulation of the averaged mixing effect of the eddies. Unfortunately, the frequency of measurement in the Steinfeldt and Rhein [17] data is insufficient to distinguish any low frequency modulation of net-eddy effects from the high-frequency signals of individual eddies.

Several studies have pointed out the presence of a DWBC bifurcation near the equator into an eastward and a southward branches [22]. Although the exact location and extent of the bifurcation are still under debate (e.g., [1]), Steinfeldt and Rhein [17] see some evidence of this circulation feature for LNADW from the equator at 35°W to 10°S. This introduces a third additional possible mechanism to temporal tracer fluctuations, i.e., that these can be driven by temporal variability in the proportion of the DWBC that heads East, rather than that continues South (to 10°S). Although a quantitative study of the bifurcation of the DWBC is of considerable interest, we do not address it here. This analysis should be viewed as a first attempt to quantify tracer-fluctuations mechanisms. In this spirit, each of the 1D models presented in this work could be separately applied to each branch of the DWBC.

Finally, we have assumed a linearly increasing boundary condition to obtain the analytic solutions for the perturbed models. In reality, increasing anthropogenic tracers (e.g., CFCs and anthropogenic CO<sub>2</sub>) have surface-water time variations that vary considerably from linearity. Anthropogenic CO<sub>2</sub> has increased approximately exponentially. CFCs had increased exponentially, until leveling in the late 1990s. Nonetheless, linearity offers a first approximation over one or two decades and permits us to solve the models and obtain at least a qualitative description of the effects of transport variations acting on background tracer gradients. In this way, competing explanations for observed tracer variability (variations in formation rates versus variations in transport) can be tested. Here, we are interested in basic testing of mechanisms, sensitivity to parameters and qualitative comparison to observations. For more detailed studies of tracer variations, numerical solutions to the advection–diffusion and/or advection–dilution models could be obtained using more realistic tracer boundary conditions and transport fluctuations. For example, the technique to estimate anthropogenic CO<sub>2</sub> uptake in the Labrador Sea by Terenzi et al. [19], which uses a steady-state advection–diffusion model and is driven by observed atmospheric carbon history, could be generalized to include decadal transport variations. In stratospheric tracer analysis, the effects of transport variations due to natural mechanisms (e.g., quasi-biennial oscillation) and anthropogenic mechanisms (e.g., secular changes in the Brewer–Dobson circulation associated with greenhouse forcing) on the mean-age in the tropical stratosphere could be elucidated with models similar to those presented here.

## 4 Conclusions

The use of 1D advection–diffusion and advection–dilution (boundary-current) models to interpret tracer observations is ubiquitous in ocean and atmosphere science. As far as we know, these models are always applied using transport coefficients that are constant in time, despite the fact that the real system under study is often clearly variable. Constant coefficients provide a zero-order view of the system, a convenient translation of tracer concentrations to rough transport timescales. However, as we show here, these simple models can be

solved analytically with small-amplitude time-varying coefficients using standard methods. A primary goal of this work has been to present and document such solutions in the hope that they may be of use to researchers who want to go one step beyond the simplest analysis, while still maintaining the convenience and ease of a low-parameter analytical model.

With this goal in mind, we have solved the 1D advection–diffusion and advection–dilution models analytically with time-varying transport coefficients in a semi-infinite domain. A background (zero-order) tracer gradient is established by a linearly increasing concentration boundary condition at the origin. The time variations in transport, assumed uniform in space, act on this background gradient, resulting in fluctuations in tracer concentration. We have analyzed these fluctuations, documenting their amplitude and phase as functions of model parameters. We have also compared these transport-induced tracer fluctuations to fluctuations that can arise from a distinct mechanism: fluctuations in concentration at the boundary, propagated by time-independent transport. We find that, in regions close to the boundary, the propagated fluctuations have larger amplitude, while further downstream the transport-induced fluctuations dominate.

The comparison of propagated- to transport-induced fluctuations is relevant to a key application of the model that we report here: the interpretation of fluctuations in tracer concentrations in the sub-tropical and tropical Atlantic Deep Western Boundary Current (DWBC). Waugh and Hall [21] were able to model well the tracers CFCs, helium–tritium and SF<sub>6</sub> in the North Atlantic using a boundary-current model with constant coefficients. However, they noted that fluctuations in temperature and salinity could not be replicated by the model, which rapidly attenuated any periodic signal specified at the northern outcrop boundary. Similarly, Steinfeldt and Rhein [17] were able to reproduce averaged concentrations and trends in time series of tropical DWBC CFCs using a 1D advection–diffusion model with constant coefficients and a northern-outcrop boundary condition. However, they were not able to reproduce fluctuations in the CFCs.

We have applied the boundary-current model to the tropical DWBC CFC time series of Steinfeldt and Rhein [17]. We find that with the best-estimate parameter values of Waugh and Hall [21], transport-induced fluctuations dominate over propagated fluctuations at these distances from the northern outcrop. The propagated fluctuations are negligible and cannot explain the observed CFC fluctuations. In fact, some of the observed fluctuations are too large even to be explained by the transport fluctuation mechanism. However, other CFC fluctuations can be explained by the mechanism using plausible parameter values.

**Acknowledgements** We thank Darryn Waugh for useful discussions and comments and Reiner Steinfeldt for providing CFC data that allowed a comparison between observational data and model results. Finally, we are grateful to two anonymous reviewers whose comments lead to a much improved manuscript. This work was supported by NSF Award OCE-06-23366.

## Appendix

In what follows we describe in some detail the procedure to find the analytical solutions for Eqns. (5) and (6) for the perturbed advection–diffusion and advection–dilution problems (1). Also, the steady-state case of a periodical boundary condition is treated.

### A Solutions for a linear varying BC and fluctuation in transport

In order to solve Eq. (1) analytically, we perform a perturbation of order  $O(\epsilon)$ ; that is, we consider solutions of the form  $\mathbf{c} = \mathbf{c}^{(0)} + \epsilon \mathbf{c}^{(1)}$ . Eq. (1) is separated into zero-th and first-order components. The zero-th order component is

$$\frac{\partial \mathbf{c}^{(0)}}{\partial t} + \mathbf{L}(\mathbf{c}^{(0)}) = \mathbf{0}, \tag{11}$$

while the first-order solution satisfies the following PDE:

$$\frac{\partial \mathbf{c}^{(1)}}{\partial t} + \mathbf{L}(\mathbf{c}^{(1)}) = -f(t) \mathbf{L}(\mathbf{c}^{(0)}). \tag{12}$$

The initial condition is  $\mathbf{c}^{(i)} = 0$  at  $t = 0$  for both  $i = 0, 1$ . The zero-th order BC at  $x = 0$  is  $\mathbf{c}^{(0)} = \mathbf{y}(t)$  and  $\mathbf{c}^{(1)} = 0$ . Note that the first-order equation is equivalent to the zero-th order equation, except for the addition of the forcing term  $-f(t) \mathbf{L}(\mathbf{c}^{(0)})$ , which depends on the zero-th order solution only. Physically, the transport variations act on the zero-th order tracer gradients to force the first-order tracer fluctuations.

Solutions to Eqs. (11) and (12) can be written as

$$\mathbf{c}^{(0)}(x, t) = \int_{-\infty}^t dt' \mathbf{y}(t') \mathbf{G}^{(0)}(x, t; t') \tag{13}$$

and

$$\mathbf{c}^{(1)}(x, t) = \int_{-\infty}^t dt' \int_0^{\infty} dx' \mathbf{F}(x', t') \mathbf{G}^{(1)}(x, t; x', t'), \tag{14}$$

where  $\mathbf{F}(x, t) = -f(t) \mathbf{L}(\mathbf{c}^{(0)}) = f(t) \frac{\partial}{\partial t} \mathbf{c}^{(0)}$  and  $\mathbf{G}^{(0)}$  and  $\mathbf{G}^{(1)}$  are the Green's functions for the respective PDEs (see Appendix B).

*Linear varying boundary condition and periodic fluctuation in transport.* We consider a linearly increasing BC,  $\mathbf{c}^{(0)}(0, t) = \mathbf{y}(t) = \gamma t$  and a periodic fluctuation in transport  $f(t) = \text{Re}(e^{i(\omega t)})$ . We assume that the BC has been present for sufficiently long that we can neglect transients in the zero-th order solution for all  $x$  of interest, and the long-time solution is given by Eq. (5). For the advection–diffusion model the mean transit time is simply the advective time, given by

$$\Gamma = \tau_{\text{adv}} = \frac{x}{u}. \tag{15}$$

For the boundary-current model

$$\begin{cases} \Gamma_b = \tau_{\text{adv}} \left(1 + \frac{1}{\alpha}\right), \\ \Gamma_i = \Gamma_b + \frac{\tau_{\text{mix}}}{\alpha}, \end{cases} \tag{16}$$

(see [21]). In this case, the forcing term in Eq. (14) becomes:

$$\mathbf{F} = f(t) \frac{\partial \mathbf{c}^{(0)}}{\partial t} = \gamma \text{Re}\left(e^{i(\omega t)}\right). \tag{17}$$

We now turn to the solutions  $\mathbf{c}^{(1)}$  in (6) for the 1D advection–diffusion and boundary-current models.

### A.1 1 D Advection–diffusion model

The solution  $\mathbf{c}^{(1)}$  is

$$c^{(1)}(x, t) = \text{Re} \left\{ \int_0^\infty dx' \int_{-\infty}^t dt' \gamma e^{i\omega(t-t')} G^{(1)}(x, t; x', t') \right\} = \gamma \text{Re} \left\{ e^{i\omega t} |I| e^{-i\phi} \right\}. \tag{18}$$

with  $G^{(1)}$  given by Eq. (38) and

$$I = \int_0^\infty dx' \int_{-\infty}^t dt' e^{-i\omega t'} G^{(1)}(x, t; x', t') = I_R - iI_C = |I| e^{-i\phi}, \tag{19}$$

where  $|I| = \sqrt{I_R^2 + I_C^2}$ , and  $\tan \phi = \frac{I_C}{I_R}$ . In order to solve the above integral, the “trick” is to recast and regroup the exponential arguments in Eq. (38) for both  $x < x'$  and  $x > x'$ , so that the exponent in time has the form  $-\left(\frac{u^2}{4k} + i\omega\right)t'$ . We then recognize that the resulting integrand is a Laplace transform with complex Laplace variable  $s = \left(\frac{u^2}{4k} + i\omega\right)$  and find the transform from standard tables. Finally (18) can be expressed as

$$c^{(1)}(x, t) = A^{(1)}(x) \cos \left( \omega \left( t - \tau^{(1)}(x) \right) \right), \tag{20}$$

where

$$A^{(1)}(x) = \gamma |I| \tag{21}$$

and

$$\tau^{(1)}(x) = \frac{\phi}{\omega}. \tag{22}$$

In the above expressions  $I_R = [E_-(x) - E_+(x)] - [E_-(0) - E_+(0)]$ ,  $I_C = [O_-(x) - O_+(x)] - [O_-(0) - O_+(0)]$ , with

$$\begin{Bmatrix} E_{-,+}(x) \\ O_{-,+}(x) \end{Bmatrix} = \frac{1}{2k\sqrt{|\frac{s}{k}|} |Z_{-,+}|} e^{a-x} \begin{Bmatrix} \cos \left( bx + \frac{\theta}{2} + \alpha_{-,+} \right) \\ \sin \left( bx + \frac{\theta}{2} + \alpha_{-,+} \right) \end{Bmatrix}. \tag{23}$$

Here,  $a_{-,+} = \frac{u}{2k} \mp \sqrt{|\frac{s}{k}|} \cos \frac{\theta}{2}$ ,  $b = \sqrt{|\frac{s}{k}|} \sin \frac{\theta}{2}$ , and  $\alpha_{-,+} = \arctan \left( \mp \frac{b}{a_{-,+}} \right)$ , with  $Z_{-,+} = \frac{u}{2k} \mp \sqrt{\frac{s}{k}}$ , where:  $\sqrt{\frac{s}{k}} = \sqrt{|\frac{s}{k}|} e^{i\frac{\theta}{2}}$ ,  $|\frac{s}{k}| = \sqrt{\left(\frac{u}{2k}\right)^4 + \left(\frac{\omega}{k}\right)^2}$ , and  $\theta = \arctan \left( \frac{4k\omega}{u^2} \right)$ .

### A.2 Boundary-current model

The expressions for the components of  $\mathbf{c}^{(1)}$  become:

$$c_b^{(1)} = \gamma \text{Re} \left( \int_0^\infty dx' \int_{-\infty}^t dt' e^{i\omega t'} (G_{bb}^{(1)} + G_{bi}^{(1)}) \right) \tag{24}$$

$$c_i^{(1)} = \gamma \text{Re} \left( \int_0^\infty dx' \int_{-\infty}^t dt' e^{i\omega t'} (G_{bi}^{(1)} + G_{ii}^{(1)}) \right). \tag{25}$$

The time integrals can be evaluated by changing the time variable to  $t'' = t - t'$ , grouping terms so that the exponent has the form  $-(\alpha\sigma + i\omega)t''$ , recognizing the resulting integrand as

a Laplace transform with complex Laplace variable  $s = \alpha\sigma + i\omega$  and finding the transform in standard tables. (For transforming the term in  $I_1$  we exploit  $I_1(y) = \frac{d}{dy}I_0(y)$  and the rule for Laplace transforms of derivatives.) The remaining  $x$  integrand is comprised solely of simple exponentials. The result for the boundary-current region is

$$c_b^{(1)}(x, t) = A_b^{(1)}(x) \cos\left(\omega(t - \tau_b^{(1)}(x))\right), \tag{26}$$

where the amplitude

$$A_b^{(1)} = \frac{\gamma}{\omega} \left(1 + e^{-2\sigma\beta-x/u} - 2e^{-\sigma\beta-x/u} \cos(\omega\beta+x/u)\right)^{1/2}, \tag{27}$$

the phase-lag time

$$\tau_b^{(1)} = -\frac{1}{\omega} \arctan\left(\frac{C_2(1 - e^{-\sigma\beta-x/u} \cos(\omega\beta+x/u)) + C_1e^{-\sigma\beta-x/u} \sin(\omega\beta+x/u)}{C_1(1 - e^{-\sigma\beta-x/u} \cos(\omega\beta+x/u)) - C_2e^{-\sigma\beta-x/u} \sin(\omega\beta+x/u)}\right), \tag{28}$$

with

$$C_1 = \sigma^2\omega^2 - (\omega^2 + \alpha^2\sigma^2 + \alpha\sigma^2)^2 \tag{29}$$

$$C_2 = 2\sigma\omega(\omega^2 + \alpha^2\sigma^2 + \alpha\sigma^2), \tag{30}$$

and

$$\beta_{\pm} = 1 \pm \frac{\alpha^2\sigma^2}{\omega^2 + \alpha^2\sigma^2}. \tag{31}$$

The interior region solution  $c_i^{(1)}$  has the following simple phase and amplitude relation to  $c_b^{(1)}$ :

$$A_i^{(1)} = \frac{\alpha\sigma}{\sqrt{\omega^2 + \alpha^2\sigma^2}} A_b^{(1)} \tag{32}$$

and

$$\tau_i^{(1)} = \tau_b^{(1)} - \frac{1}{\omega} \arctan\left(\frac{\omega}{\alpha\sigma}\right). \tag{33}$$

### B Green’s functions

The Green’s functions that appear in Eqs. (13) and (14) are the solutions to

$$\frac{\partial \mathbf{G}^{(k)}}{\partial t} + \mathbf{L}(\mathbf{G}^{(k)}) = \mathbf{S}^{(k)}, \tag{34}$$

with index  $k = 0, 1$ . For the zero-th order solution,  $\mathbf{S}^{(0)} = 0$ ,  $\mathbf{G}^{(0)}(x, 0) = 0$ , and  $\mathbf{G}^{(0)}(0, t) = \delta(t)$ ; For the first-order solution,  $\mathbf{S}^{(1)} = \mathbf{I} \cdot \delta(t - t') \delta(x - x')$ , where  $\mathbf{I}$  is the identity matrix;  $\mathbf{G}^{(1)}$  satisfies both homogeneous boundary and initial conditions.

For the advection–diffusion model the solution has only one component,  $\mathbf{G}^{(k)} = \mathbf{G}^{(k)}(\mathbf{x}, \mathbf{t}|\mathbf{x}', \mathbf{t}')$ . For the boundary-current model we have

$$\mathbf{G}^{(0)} = \begin{pmatrix} G_b^{(0)}(x, t|x', t') \\ G_i^{(0)}(x, t|x', t') \end{pmatrix} \tag{35}$$

and

$$\mathbf{G}^{(1)} = \begin{pmatrix} G_{bb}^{(1)}(x, t|x', t') & G_{bi}^{(1)}(x, t|x', t') \\ G_{ib}^{(1)}(x, t|x', t') & G_{ii}^{(1)}(x, t|x', t') \end{pmatrix}. \tag{36}$$

For instance, the matrix element  $G_{bi}^{(1)}(x, t|x', t')$  is the response at time  $t$  and position  $x$  in the boundary-current core region to a point source at a previous time  $t'$  and position  $x'$  in the surrounding interior region.

**B.1 1 D Advection–diffusion Model**

*B.1.1 Zero-th order solution*

$$G^{(0)}(x, t|t') = \frac{x}{\sqrt{4\pi k(t-t')^3}} e^{-\frac{(x-u(t-t'))^2}{4kt}} \tag{37}$$

*B.1.2 First-order solution*

$$G^{(1)}(x, t|x', t') = \frac{1}{\sqrt{4k\pi(t-t')}} e^{-\frac{u(x'-x)}{2k}} e^{-\frac{u^2(t-t')}{4k}} \begin{cases} e^{-\frac{(x'-x)^2}{4k(t-t')}} - e^{-\frac{(x'+x)^2}{4k(t-t')}} & x < x' \\ e^{-\frac{(x-x')^2}{4k(t-t')}} - e^{-\frac{(x+x')^2}{4k(t-t')}} & x > x' \end{cases} \tag{38}$$

**B.2 Boundary-current model**

*B.2.1 Zero-th order solution*

Waugh and Hall [21] found that:

$$G_b^{(0)}(x, t) = \widehat{G}_1 \delta(t - \tau_{adv}) + \widehat{G}_2 \Theta(t - \tau_{adv}) \tag{39}$$

and

$$G_i^{(0)}(x, t) = \widehat{G}_3 \Theta(t - \tau_{adv}) \tag{40}$$

where

$$\widehat{G}_1 = \exp^{-\frac{1}{Pe}}, \quad \widehat{G}_2 = \frac{\alpha}{\zeta \tau_{mix}} \exp^{-\frac{1 + \zeta^2}{Pe}} I_1\left(\frac{2\zeta}{Pe}\right),$$

$$\widehat{G}_3 = \frac{\alpha}{\tau_{mix}} \exp^{-\frac{1 + \zeta^2}{Pe}} I_0\left(\frac{2\zeta}{Pe}\right)$$

$\tau_{adv} = \frac{x}{u}$ ,  $Pe = \frac{\tau_{mix}}{\tau_{adv}}$ ,  $\zeta^2 = \alpha(\hat{t} - 1)$ ,  $\hat{t} = \frac{t}{\tau_{adv}}$ ,  $I_0$  and  $I_1$  are modified Bessel functions of zero-th and first-order.

*B.2.2 First-order solution*

$$G_{bb}^{(1)} = \frac{1}{u} \sqrt{\frac{\alpha\sigma^2(x-x')}{uT}} e^{-\frac{\sigma}{u}(x-x')} e^{-\alpha\sigma T} I_1\left(2\sqrt{\frac{1}{u}\alpha\sigma^2(x-x')T}\right) \Theta(T)$$

$$+ \frac{1}{u} e^{-\frac{\sigma}{u}(x-x')} \delta(T), \tag{41}$$

$$G_{ib}^{(1)} = \frac{\alpha\sigma}{u} e^{-\frac{\sigma}{u}(x-x')} e^{-\alpha\sigma T} I_0 \left( 2\sqrt{\frac{1}{u}\alpha\sigma^2(x-x')T} \right) \Theta(T), \tag{42}$$

$$G_{ii}^{(1)} = \sqrt{\frac{\alpha\sigma^2 T}{u(x-x')}} e^{-\sigma(x-x')T/u} e^{-\alpha\sigma T} I_1 \left( 2\sqrt{\frac{1}{u}\alpha\sigma^2(x-x')T} \right) \Theta(T), \tag{43}$$

and

$$G_{bi}^{(1)} = \frac{1}{\alpha} G_{bi}^{(1)}, \tag{44}$$

where  $T = t - t' - \frac{1}{u}(x - x')$  and  $I_n$  is the modified Bessel function of order  $n$ . Because the zero-th order transport is in steady-state, the solutions depend only on the difference  $t - t'$ .

### C Solutions for a periodic tracer BC

In this section we give the solutions to the steady-state versions of the two models where periodic BCs apply. The solutions can be written as  $c(x, t) = P(x) \cos(\omega(t - \phi(x)))$ . For the advection–diffusion model

$$P(x) = P_0 \sqrt{\mathcal{P}_R^2 + P_C^2}, \tag{45}$$

$$\phi(x) = \frac{1}{\omega} \cdot \frac{P_C}{P_R} \tag{46}$$

$P_R = e^{Z_R x} \cos(Z_C x)$  and  $P_C = e^{Z_R x} \sin(Z_C x)$ , where  $Z_R \equiv a_-$  and  $Z_C \equiv b$ , with  $a_-$  and  $b$  given in (A.1). For the boundary-current model the solution in the core region is given by

$$P(x) = P_0 \exp\left(-\frac{x\sigma\omega^2}{u(\omega^2 + \alpha^2\sigma^2)}\right) \tag{47}$$

$$\phi(x) = \frac{x}{u} \cdot \frac{\omega^2 + \alpha(\alpha + 1)\sigma^2}{\omega^2 + \alpha^2\sigma^2} \tag{48}$$

(see [21]).

### References

1. Andrie C, Terson JF, Messias MJ, Memery L, Bourles B (1998) Chlorofluoromethane distributions in the deep equatorial atlantic during january-march 1993 - water masses and transports near the equator. *Deep Sea Res I* 45:903–930(28)
2. Curry RG, McCartney MS, Joyce TM (1998) Oceanic transport of subpolar climate signals to mid-depth subtropical waters. *Nature* 391:575–577
3. Doney SS, Jenkins WJ (1994) Ventilation of the deep western boundary current and abyssal western North Atlantic: estimates from tritium and <sup>3</sup>He distributions. *J Phys Oceanogr* 24:638–659
4. Freudenthal S, Andrie C (2002) The arrival of a “new” Labrador Sea Water signal in the tropical Atlantic in 1996. *Geophys Res Lett* 29(15): 1741. doi:10.1029/2002GL015062
5. Haine TW, Watson AJ, Liddicoat MI, Dickson RR (1998) The flow of Antarctic bottom water to the southwest Indian Ocean estimated using CFCs. *J Geophys Res* 103(C12):27637–27654
6. Hall TM, Haine TW, Waugh DW (2002) Inferring the concentration of anthropogenic carbon in the ocean from tracers. *Glob. Biogeochem. Cycles* 16(4):1131. doi:10.1029/2001GB001835
7. Hall TM, Waugh DW (2000) Stratospheric residence time and its relationship to mean age. *J Geophys Res* 105:6773–6782

8. Johnson GC, Bullister JL, Gruber N (2005) Labrador Sea Water property variations in the northeastern Atlantic Ocean. *Geophys Res Lett* 32:L07602
9. McKenna DS (1997) Analytic solutions of reaction diffusion equations and implications for the concept of an air parcel. *J Geophys Res* 102(D):13719–13725
10. Molinari RL, Fine RA, Wilson WD, Curry RG, Abell J, McCartney MS (1998) The arrival of recently formed Labrador Sea water in the deep western boundary current at 26.5°N. *Geophys Res Lett* 25:2249–2252
11. Mote PW, Dunkerton TJ, McIntyre ME, Ray EA, Haynes PH, J MRIII (1998) Vertical velocity, vertical diffusion, and dilution by midlatitude lower stratosphere. *J Geophys Res* 103(D8):8651–8666
12. Mouchet A, Deleersnijder E (2008) The leaky funnel model, a metaphor of the ventilation of the World Ocean as simulated in an OGCM. *Tellus A* 60:761–774
13. Neu J, Plumb AR (1999) Age of air in a “leaky pipe” model of stratospheric transport. *J Geophys Res* 104:19243–19255
14. Pickart R, Hogg N, Smethie WM (1989) Determining the strength of the deep western boundary current using the chlorofluoromethane ratio. *J Phys Oceanogr* 19:940–951
15. Plumb AR (1996) A tropical pipe model of stratospheric transport. *J Geophys Res* 101:3957–3972
16. Rhein M (1994) The deep western boundary current—tracers and velocities. *Deep Sea Res* 41:263–281
17. Steinfeldt R, Rhein M (2004) Spreading velocities and dilution of North Atlantic deep water in the tropical Atlantic based on CFC time series. *J Geophys Res* 109:C03046.
18. Sunnerup RE (2001) On the relations among CFC derived water mass ages. *Geophys Res Lett* 28(9):1739–1742
19. Terenzi F, Hall TM, Khatiwala S, Rodehacke CB, LeBel DA (2007) Uptake of natural and anthropogenic carbon by the Labrador Sea. *Geophys Res Lett* 34:L06608
20. Waugh DW, Hall TM (2002) Age of stratospheric air; theory, observations, and models. *Rev Geophys* 40(4):1010
21. Waugh DW, Hall TM (2005) Propagation of tracer signals in boundary currents *J Phys Oceanogr* 35: 1538–1552. doi:[10.1175/JPO2779.1](https://doi.org/10.1175/JPO2779.1)
22. Weiss RF, Bullister JL, Gammon RH, Warner MJ (1985) Atmospheric chlorofluoromethanes in the deep equatorial Atlantic. *Nature* 314:608–610